JOURNAL OF GEOPHYSICAL RESEARCH, VOL. 113, D16205, doi:10.1029/2007JD009384, 2008

Seasonal statistical characteristics of aerosol optical properties at a site near a dust region in China

Youfei Zheng,[1] Jianjun Liu,[1] Rongjun Wu,[1] Zhanqing Li,[1,2] Biao Wang,[3] and Takamura Tamio[4]

Received 12 September 2007; revised 6 February 2008; accepted 4 April 2008; published 22 August 2008.

[1] A ground-based sky radiometer was used to measure direct and diffuse solar irradiances at Dunhuang, China from January 1999 to March 2001. The aerosol optical thickness (AOT), Angstrom exponent (α), volume size distributions, single scattering albedo and refractive index of aerosols were simultaneously retrieved using the "SKYRAD" inversion code and their seasonal variations and statistical characteristics were studied. The results reveal that during the study period, the AOT at Dunhuang varied seasonally, with the maximum AOT occurring in the spring and the minimum AOT occurring in the fall. The variation in α showed an opposite pattern, with a minimum in the spring and a maximum in the fall. A simple exponential function can express the relationship between AOT and α. The frequency distributions of AOT and α approximately follow a lognormal probability distribution and a normal probability distribution, respectively. The aerosol volume size distributions can be characterized by the sum of two lognormals distributions, and represent an accumulation mode with a radius of about 0.25 um, and a coarse mode with a radius of about 7.7 um. A pseudomode with a radius of about 1.69 um located between the accumulation mode and coarse mode is present in the springtime. The single scattering albedo showed a slight increasing trend with wavelength in spring, summer and autumn and a decreasing trend with wavelength in winter. The maximum value of the real part of the refractive index occurs at 400 nm, and the minimum value occurs at 875 nm for all seasons. Two Gaussian models were developed to describe the frequency distribution of the real part of the aerosol refractive index; the results indicate that the differences between the fits are greatest in the spring. The statistical characteristics of the frequency distributions of aerosol properties might provide a way to identify and estimate aerosol optical properties in areas located near dust regions.

Citation: Zheng, Y., J. Liu, R. Wu, Z. Li, B. Wang, and T. Tamio (2008), Seasonal statistical characteristics of aerosol optical properties at a site near a dust region in China, *J. Geophys. Res.*, *113*, D16205, doi:10.1029/2007JD009384.

1. Introduction

[2] Atmospheric aerosols are one of the most variable components of the Earth's atmospheric environment, which can affect and change the Earth-atmosphere system's radiation budget through direct effects, semidirect effects, the cloud albedo effect (1st indirect effect) and the cloud lifetime effect (2nd indirect effect) [*IPCC*, 2007]. Many studies regarding spatial and temporal variations of atmospheric aerosols have been carried out [*Xia et al.*, 2004, 2007; *Wang et al.*, 2006; *Chen et al.*, 2007; *Kaufman et al.*, 2002; *Dubovik et al.*, 2002; *William et al.*, 2007; *Behnert et al.*, 2007], but considerable uncertainties still exist due to the poor understanding of aerosol properties [*Schwartz and Andreae*, 1996; *IPCC*, 2001, 2007; *AMS*, 2003].

[3] Ground-based remote sensing of aerosols is ideal for the reliable and continuous derivation of aerosol properties in key locations around the world. An advantage of this ground-based perspective is that the retrievals are representative for the entire vertical column with no height dependence, which is particularly true for the refractive indices and the parameters of the particle size distribution. Ground-based measurements of a variety of optical aerosol characteristics are necessary for validating aerosol products obtained from various satellite sensors [*Li et al.*, 2007]. Many aerosol ground-based observation networks have been established in order to understand and evaluate optical properties and their effects on climate; they include AERONET (An Automatic Robotic Sun and Sky Scan-

[1]College of Environmental Science and Engineering, Nanjing University of Information Science and Technology, Nanjing, China.
[2]Department of Atmospheric and Oceanic Science and Earth System Science Interdisciplinary Center, University of Maryland, College Park, Maryland, USA.
[3]Institute of Atmospheric Physics, Chinese Academy of Sciences, Beijing, China.
[4]Center for Environmental Remote Sensing, Chiba University, Chiba, Japan.

0148-0227/08/2007JD009384$09.00

ning Measurement Program) [*Holben et al.*, 1998, 2001], SKYNET (A Sun and Sky Radiometer Network Based in East-Asia) [*Takamura et al.*, 2002], GAW (Global Atmosphere Watch Programme) [*WMO*, 2001], and the Chinese Sun Hazemeter Network [*Xin et al.*, 2006].

[4] Aerosols are not well-mixed in the atmosphere so their properties, such as the optical thickness (AOT) and the Angstrom exponent (α),depend on geographic scenarios that govern the emission, transport, atmospheric transformation and removal of aerosol particles. Given the short lifetime of aerosol particles, their properties vary with time and from one region to another. Dunhuang (DH; latitude: 94.802°E, longitude: 40.163°N, altitude: 1120 m) is located at the west end of the Hexi Corridor in the Gansu province of China, which is an area where there is much dust activity. Because of its location and the establishment of a good infrastructure, DH has been selected as a supersite for many international aerosol field experiments such as the Aerosol Characterization Experiment-Asia (ACE-Asia), and the China and Japan joint plan on Aeolian dust effect son climate (ADEC) Understanding how AOT varies locally would improve the current knowledge about aerosols around the world and would be useful in integrating global data sets as suggested by *Charlson* [2000]. Also, some authors [*King et al.*, 1980; *Ignatov and Stowe*, 2000; *O'Neill et al.*, 2000] have indicated that the statistical characteristics of AOT are also important in estimating aerosol optical properties accurately and completely.

[5] To date, the statistical characteristics of other aerosol optical properties have not been thoroughly studied. This paper attempts to rectify this situation through the statistical analysis of retrievals of aerosol optical thickness, Angstrom exponent, size distribution, single scattering albedo, as well as the real and imaginary parts of the refractive index, obtained at DH from direct and diffuse solar irradiance measurements. Section 2 describes the sky radiometer and its calibration. The data and methods used in the analysis are outlined in section 3 and section 4 presents the results. Conclusions are given in section 5.

2. Instrument and Calibration

[6] The ground-based sky radiometer (POM-01; manufactured by Prede Co., Ltd., Tokyo, Japan) is a portable instrument that can measure direct and diffuse solar irradiances, as well as the aureole in the solar almucantar and the principal plane under daytime clear-sky conditions. The instrument is based on the aureolemeter [*Shiobara et al.*, 1991] and is composed of a sun- and sky-scanning spectral radiometer, a sun sensor, a sun tracker, a control unit, a rain sensor, and a personal computer. There are seven filters with central wavelengths at 315, 400, 500, 675, 870, 940, and 1020 nm; the half-bandwidth wavelength at 315 nm is 3 nm and less than 10 nm at the other wavelengths. Measurements made at 315 and 940 nm are used for deriving the O_3 concentration and precipitable water column amounts, respectively; measurements at the other wavelengths are used for aerosol remote sensing. The field of view is 1° and the minimum angle for sky measurements is about 3°. The sky radiometer is mounted on a vertical-horizontal two-axes mount that is driven by digital servomotors for scanning sky radiation distributions. The detector sensitivity is strongly dependent on temperature, so the detector temperature is kept constant at 30°C. A preprogrammed sequence of measurements is taken by the aureolemeter: during periods when the air mass is larger than 3, solar direct and diffuse measurements are made at about 0.25 air mass intervals, while at smaller air masses, the sampling interval is typically 10 min. Details of the scanning method can be found by *Tonna et al.* [1995].

[7] Accurate calibration of the radiometer constant, $V_{0,\lambda}$, is essential in ground-based measurements [*Schmid et al.*, 1998]. The accuracy with which AOTs can be retrieved depends mainly on the accuracy of the $V_{0,\lambda}$ value. $V_{0,\lambda}$ errors should be less than 2% in order to obtain AOTs with an uncertainty less than 0.02 when the air mass is equal to 1. The Langley method (LM), a straightforward application of the Bouguer-Lamber-Beer law, is practically the de facto standard, owing to its high accuracy and its convenient application in the field. However the assumption that the atmosphere remains stable during the calibration period of one to several hours, is not satisfied at most locations and under most situations. Accordingly, some modified Langley methods (MLMs) have been developed [*Tanaka et al.*, 1986; *O'Neill and Miller*, 1984], in which the temporarily variable atmospheric turbidity is taken into consideration. In this paper, the radiometer was calibrated using the modified Langley method suggested by *Nakajima et al.* [1996], which is an extension of Tanaka et al.'s MLM. The first step involves performing an inversion with only forward scattering intensity data (3°–40°), from which temporarily variable AOT are derived. There are two reasons for only considering forward scattering. One reason is that the forward scattering part of the radiation field (3°–40°) mainly consists of diffracted radiation which is mostly dependent on the scattering cross-section of particles without much dependence on the refractive index and nonsphericity of the particles. Another reason is that this part of the scattered radiation field is the circum-solar region which is generally unaffected by the inhomogeneity in the horizontal distribution of aerosols and ozone absorption. These AOT values are then multiplied by the corresponding air mass (m) and used to obtain the radiometer constant (F0) through the Lambert Beer's equation: $\ln(F) = \ln(F0) - m*AOT$. In this process, AOT can be a rough estimate of atmospheric turbidity, which includes temporal changes during the period of time during which the Langley plot is generated. A sensitivity study showed that the effects of the uncertainties in the input parameters, such as refractive index, and measurement errors on calibration were weak, so a calibration accuracy of 1% can be achieved using this method. Hence the errors in AOT retrievals are approximately 0.01 at one air mass.

3. Data and Methods

3.1. Data

[8] Direct and diffuse solar irradiance measurements, as well as aureole radiance measurements, were taken at the DH site from January 1999 to March 2001. The sampling interval was 10 min from sunrise to sunset under clear-sky conditions Surface pressures needed for Rayleigh scattering optical thickness calculations were obtained from the DH meteorological observatory located near the observation station. The columnar ozone contents for ozone absorption optical

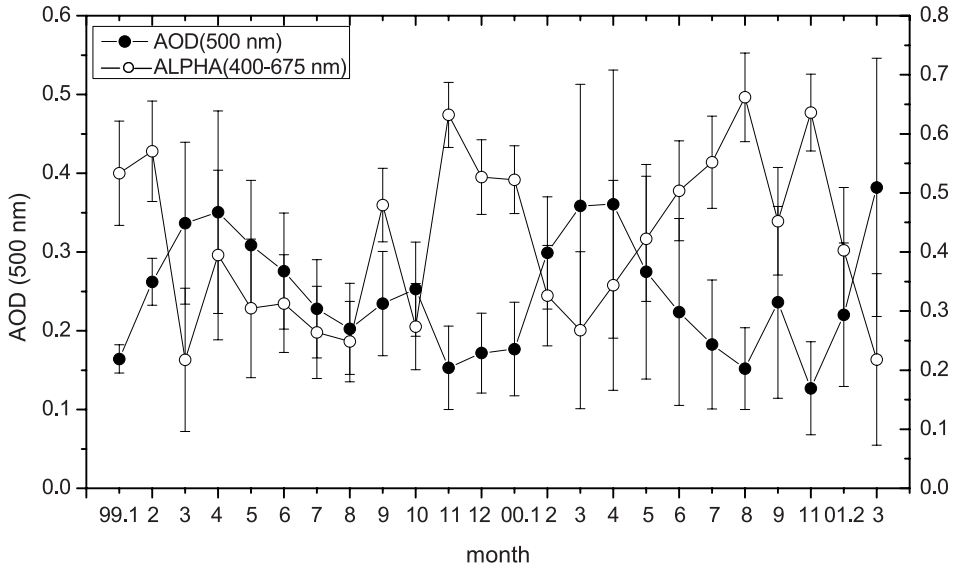

Figure 1. Time series of monthly averaged aerosol optical thickness (500 nm) and Angstrom exponent (400–675 nm).

thickness calculations were obtained from the Total Ozone Mapping Spectrometer. The surface albedos over the DH area were obtained from the MODIS surface albedo product.

3.2. Methods

[9] Aerosol properties were retrieved using the newest version (v4.2, April 2006) of the "SKYRAD" inversion code, which was developed by *Nakajima et al.* [1996]. The first step in the retrieval is the computation of direct and diffuse components of solar radiation, which is used to construct test simulation data for the inversion code; input parameters are described by *Nakajima et al.* [1996]. The second step in the retrieval is the determination of aerosol properties from solar radiation data (real or simulated). The aerosol optical depth, size distribution, single scattering albedo and refractive index can be retrieved from the observation of direct and diffuse solar irradiances, as well as aureole radiances. Its structure and inversion accuracy are discussed in detail in the literature [*Nakajima et al.*, 1996; *Tonna et al.*, 1995]. On average, the errors for the minimum and maximum size ranges (0.05–0.1 um and 7–15 um) may be as large as 35–100%, but the precision for the middle range is expected to be smaller than 20%.

[10] The Angstrom exponent is determined from the spectral dependence of the measured optical thicknesses, and is a good indicator of the aerosol size. This coefficient is computed using regression analysis, in which the AOT values for three wavelengths (400, 500, and 675 um) are fitted to the following equation:

$$\tau_a(\lambda) = \beta\lambda^{\alpha} \tag{1}$$

where λ is the wavelength, and β is the aerosol turbidity coefficient (i.e., AOT at $\lambda = 1$ um). The data for α are used only when a high correlation coefficient ($R > 0.90$) is obtained in the regression analysis using equation (1).

[11] The radiometer automatically collects data about non-precipitating sky conditions according to a preprogrammed sequence, thus, cloud screening is essential for data quality purposes. Here, the cloud screening method developed by *Smirnov et al.* [2000] and applied to AERONET data was utilized. This technique is based on the principle that clouds have larger optical thicknesses and greater temporal variances than do aerosols. In addition, manual cloud screening for questionable data was performed using weather observations from the DH observatory.

4. Results and Discussion

4.1. Aerosol Optical Thickness (AOT) and Angstrom Exponent (α)

[12] The AOT is representative of the airborne aerosol loading in the atmospheric column and is important for the identification of aerosol source regions and aerosol evolution. Figure 1 shows the monthly mean AOT at 500 nm and α (400–675 nm) for January 1999 to March 2001, with error bars showing the standard deviation of the monthly averaged value. The seasonal variation in AOT is evident with the sharpest increase in AOT occurring during the period of December to March/April; a less pronounced increase is seen from September to October. A noticeable decrease in AOT is seen during the period of May to August. The mean AOT varies on a monthly basis with the smallest values occurring in November. This variation in AOT is related to Asian dust activities. Generally speaking, the AOT values are smaller in summer and fall and bigger in spring and winter, which is similar to results reported by *Xia et al.* [2004]. Months with high mean AOT have the largest standard deviations due to the difference in aerosol concentrations between periods of normal background and dust-laden atmospheric conditions.

[13] The pattern of the monthly change in α is opposite to that of AOT. The magnitude of α is smallest during the months of March and April, which indicates that the aerosol particles are large and likely related to dust activities. Smaller

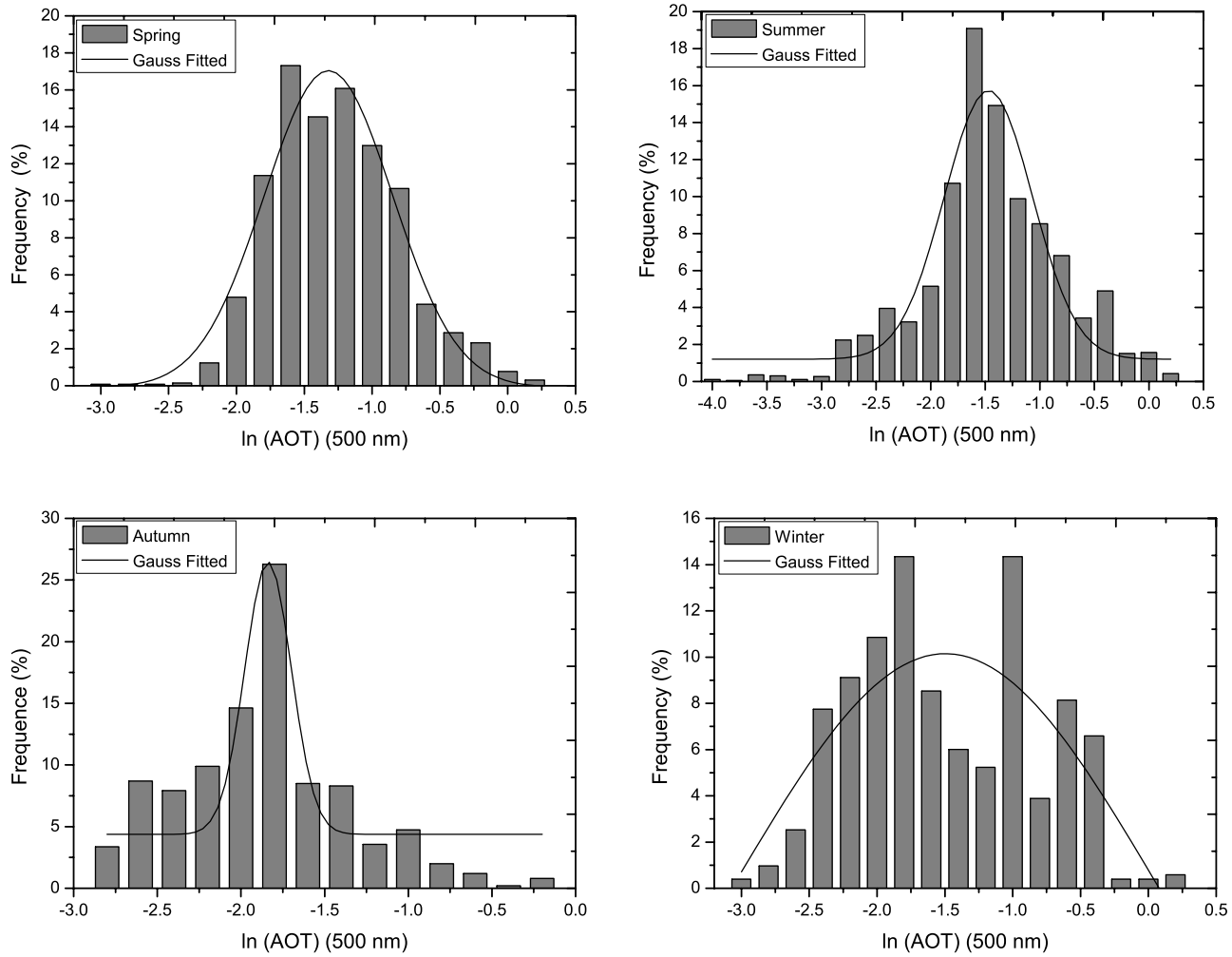

Figure 2. Frequency distributions of the aerosol optical thicknesses (500 nm) for the four seasons and the fitted Gaussian model.

aerosol particles appear to dominate in November. The standard deviations are greatest for cases when α is large.

[14] Figure 2 shows the frequency distributions of AOT (500 nm) for the four seasons. The number of samples analyzed for each season was 707 (spring), 1623 (summer), 1294 (autumn) and 917 (winter). During the spring season, more than 93% of the AOTs were larger than 0.14; approximately 17% of the AOTs ranged between 0.17–0.20 and nearly 82% of the AOTs ranged between 0.14–0.45. The frequency distribution with the widest spread occurred in the summer when 82% of the AOTs were larger than 0.14; nearly 19% of the AOTs ranged between 0.17–0.20. In the fall, more than 50% and 26% of the AOTs varied between 0.1–0.17 and 0.17–0.20, respectively. Two peaks are seen in the frequency distribution of the AOTs in winter, suggesting the complexity of the aerosol sources during this season; nearly 43% and 14% of the AOTs ranged between 0.1–0.2 and 0.3–0.7, respectively. The frequency distributions of the AOTs are consistent with their monthly variation.

[15] Previous studies have shown that the frequency distribution of AOT, or τ, can be described by the following lognormal distribution expression [*O'Neill et al.*, 2000; *Matthias and Bosenberg*, 2002; *Behnert et al.*, 2007]:

$$f(\tau) = \frac{1}{s\tau\sqrt{2\pi}} \exp\left(\frac{(\ln\tau - m)^2}{2s^2}\right).$$

[16] The data collected at DH was transformed to a logarithmic scale and fitted with the Gaussian model (thick lines in Figure 2). The form of the Gaussian model is:

$$y = y_0 + \frac{A}{w\sqrt{\pi/2}} e^{-2\frac{(x-x_c)^2}{w^2}}$$

where A is the amplitude, Xc is the center of the peak amplitude, and σ is the width at half peak amplitude. Table 1 summarizes the seasonal statistics of the AOTs based on the fitted Gaussian model. The lognormal probability distribution best represents the frequency distribution of AOTs in the spring ($R^2 = 0.959$); in winter, the fit is not so strong ($R^2 = 0.612$) because of the influence of both dust and anthropogenic aerosols So for sites near a dust region,

Table 1. Seasonal Statistics of the Aerosol Optical Thicknesses Based on the Fitted Gaussian Model

	y_0	A	x_c	w	R^2
Spring	−0.084 ± 0.676	20.292 ± 1.977	−1.322 ± 0.027	0.946 ± 0.076	0.959
Summer	1.204 ± 0.538	14.699 ± 1.655	−1.470 ± 0.038	0.807 ± 0.086	0.897
Autumn	4.379 ± 1.071	7.741 ± 1.538	−1.838 ± 0.029	0.280 ± 0.056	0.809
Winter	−15.075 ± 57.301	98.180 ± 362.361	−1.496 ± 0.111	3.106 ± 4.520	0.612

the frequency distributions of AOTs can be characterized by the lognormal probability distribution during dust events.

[17] Figure 3 shows the frequency distributions of α (400–675 nm) for the four seasons. Approximately 77% of the α values are smaller than 0.5, and nearly 22% of the values range from 0.1–0.2 during the spring season. The widest spread in the frequency distribution is seen in the summer; nearly 70% of the α values are smaller than 0.5 and about 22% of the values vary between 0.1–0.2. The magnitude of α was less than 0.5 for 52% and 62% of the fall and winter cases, respectively; 82% of the values for fall and 75% of the values for winter ranged between 0.2–0.8.

[18] The Gaussian model was used to fit the frequency distributions of α. The solid lines in Figure 3 illustrate that the frequency distributions of α follow the normal probability function to some degree; the correlation coefficients are 0.922 (spring), 0.917 (summer), 0.792 (autumn) and 0.787 (winter). This is contrary to the results presented by *Behnert et al.* [2007] in which no characteristic frequency distribution for α at various sites investigated until now was reported. The results shown in Figure 3 indicate that the frequency distributions of α at locations near dust regions, and not elsewhere, may be characterized by the normal probability distribution. A seasonal variation in Xc consistent with the variation in AOT was also found; no pattern in the variation of A and w was apparent.

[19] The dependence of α on AOT can be used to obtain the aerosol size distribution [*Fouquart et al.*, 1987; *D'almeida*, 1987]. *Cheng et al.* [2006a] studied the relationship between α and AOT at six sites in northern China in spring: Dunhuang (DH), Yulin (YL), Beijing (BJ), Xianghe (XH), Inner_Mongolia (IM), and Liaoning (LN). The results showed that given the location of the DH, YL and IM sites near dust sources, aerosol loading mainly consisted of dust particles; the relationship between α and AOT at these sites could be characterized by an integrated exponential function. A more complex scenario exists at the XH site and in particular, at the BJ and LN sites. Figure 4 shows the

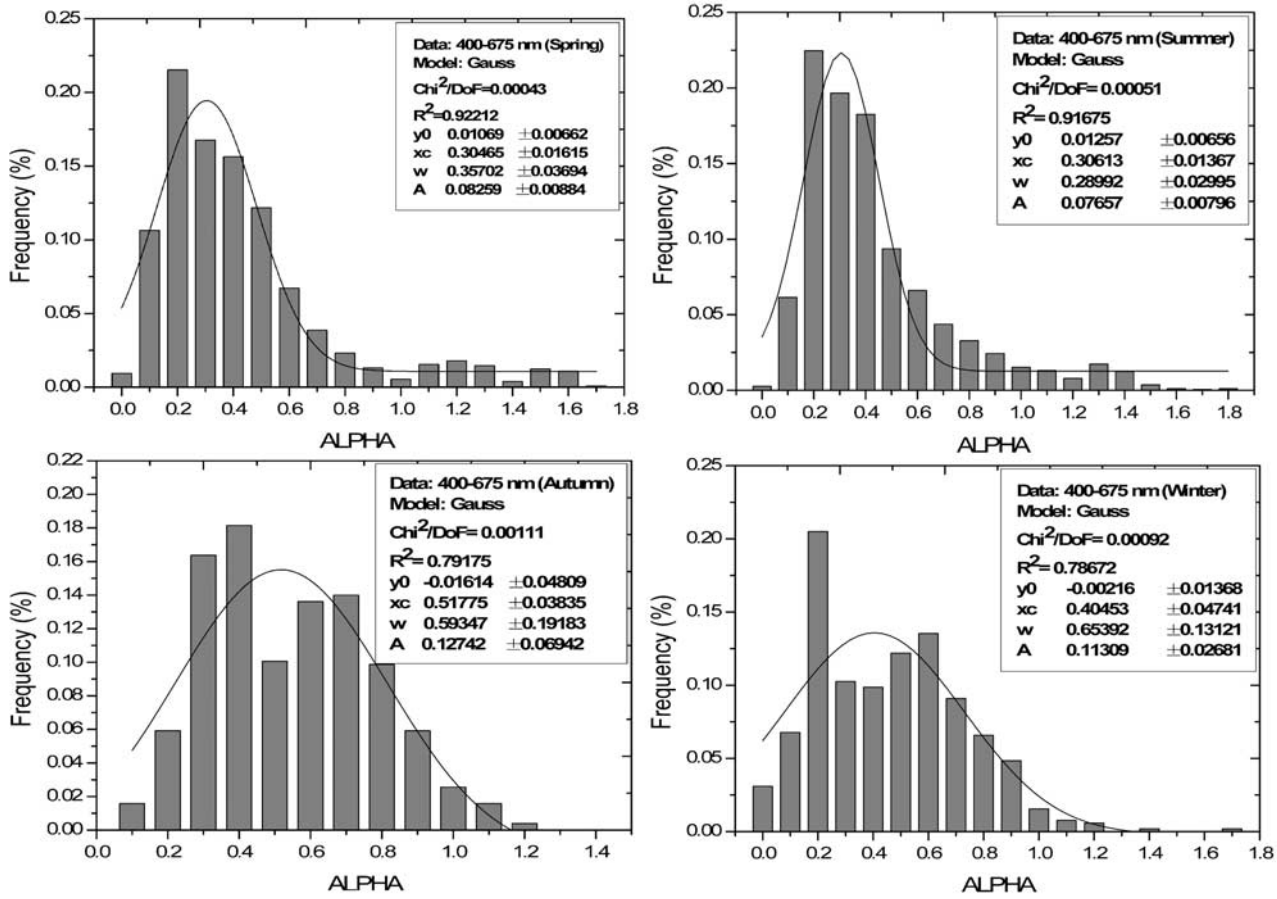

Figure 3. Frequency distributions of the Angstrom exponent for the four seasons and the fitted Gaussian model.

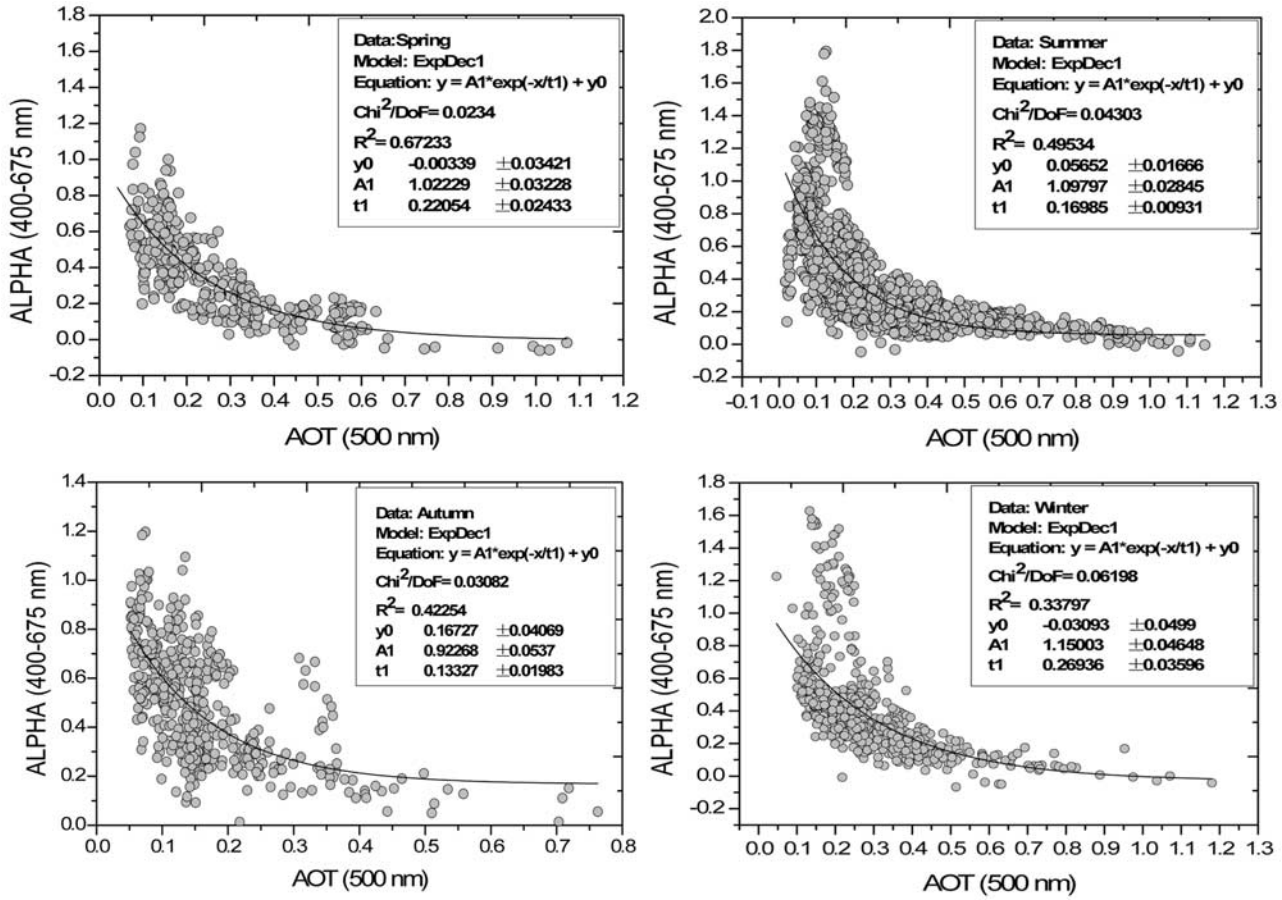

Figure 4. α (400–675 nm) as a function of AOT (500 nm) for each season.

relationship between α and AOT at DH for the four seasons and the best fit line given by a simple exponential function. In the spring, large dust particles dominate so the exponential fit is strongest during this season; the fit is weakest during the winter when the aerosol loading is more variable and when aerosols consist of a more complex combination of dust and pollutant particles. *Cheng et al.* [2006a] pointed out that this variation of the relationship between α and AOT

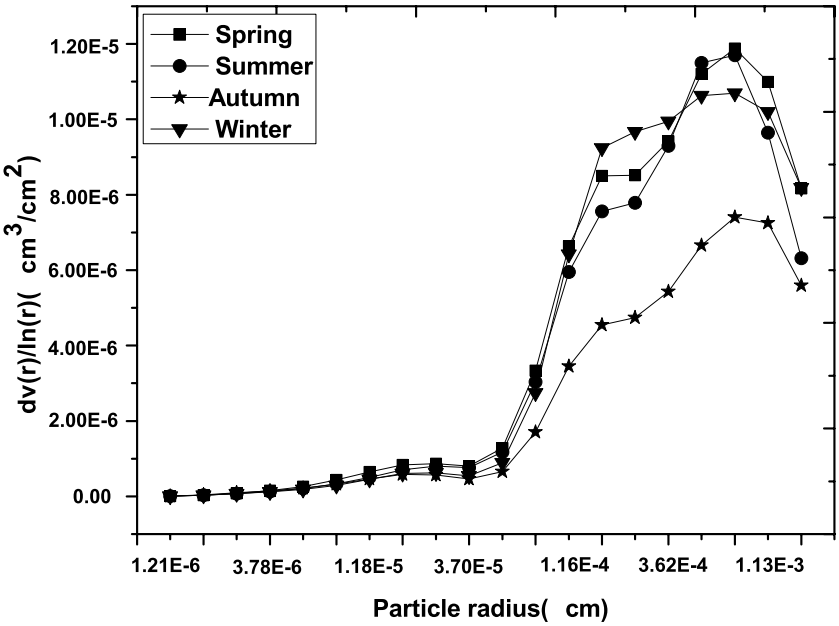

Figure 5. Seasonally averaged aerosol volume spectra (500 nm) in 20 different radius bins.

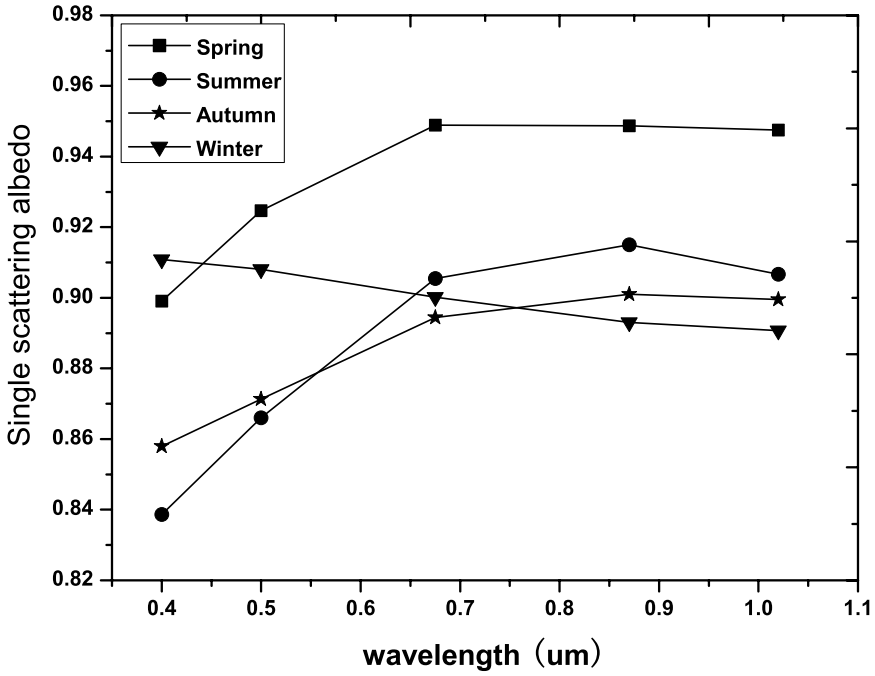

Figure 6. Seasonally averaged single scattering albedo at different wavelengths.

might provide a possible way to identify and estimate the effects of different sources on aerosol loading and aerosol size.

4.2. Aerosol Size Distribution

[20] The aerosol size distribution was determined using 20 radius size bins ranging from 10^{-6} cm to 2×10^{-3} cm. For each season, the average radius of aerosol particles in each bin was calculated. Figure 5 illustrates the seasonal variation in aerosol size. The aerosol size distribution has a two-mode structure, which can be characterized by the sum of two lognormal distributions as follows:

$$v(r) = \frac{dV(r)}{d\ln r} = \sum_{i=1}^{2} \frac{C_{v,i}}{\sqrt{2\pi}\sigma_i} \exp\left[-\frac{(\ln r - \ln r_{v,i})}{\sigma_i^2}\right],$$

where $r_{v,i}$ is the volume median radius, σ_i is the standard deviation, and $C_{v,i}$ is the volume concentration for accumulation and coarse modes [*Xia et al.*, 2005]. These integrated quantities can be approximated according to *Dubovik et al.* [2002]. One accumulation mode with a radius of about 0.25 um and varying steadily with season is seen; this is mainly related to human activities and meteorological conditions. A coarse mode with a radius of about 7.7 um is evident, as are the large variations over the seasons. The maximum value occurs in spring and the minimum value occurs in autumn, reflecting the influence of dust events. A pseudomode with a radius of about 1.69 um appears between the accumulation and coarse modes and is attributed to the high frequency of dust events in spring. There was little change in the particle volume median radius during dust and nondust periods, only changes in particle concentration.

4.3. Single Scattering Albedo

[21] The single scattering albedo, ω_o, is a common measurement of the relative contribution of absorption to extinction and is a key variable in assessing the climatic effects of aerosols [*Jacobson*, 2000; *Dubovik et al.*, 2002]. Its value is mostly dependent on the composition and size distribution of aerosol particles. The single scattering albedo of desert dust simulated according to a number of models [*Shettle and Fenn*, 1979; *WMO*, 1983; *Koepke et al.*, 1997; *Hess et al.*, 1998] ranges from 0.63 to 0.87 at 500 nm, while aircraft radiation measurements [*Fouquart et al.*, 1987] suggest lower absorption ($\omega_o = 0.95$ for the broadband solar spectrum). The main source of error in the derived single scattering albedo is due to the calibration of the radiation data, and is estimated to be ±0.03.

[22] Figure 6 shows the seasonally averaged single scattering albedo at 400, 500, 675, 870, and 1020 nm. Because of the influence of dust events during the spring, summer and autumn seasons, there was an increase in the scattering contribution of coarse particles so the single scattering albedo showed a slight increasing trend with wavelength [*Dubovik et al.*, 2002; *Xia et al.*, 2005; *Cheng et al.*, 2006b]. The variation of the single scattering albedo in winter showed a slight decrease with wavelength which is attributed to the presence of a mixture of aerosols from multiple sources. The single scattering albedo in spring was much higher than that in other seasons, with an average value of 0.934. This is slightly lower than the single scattering albedo values obtained by others for desert dust (0.95–0.99) [*Dubovik et al.*, 2002; *Kaufman et al.*, 2001], which suggests the possible combination of dust, urban-industrial particles and biomass burning aerosols over the DH area.

[23] *Lyamani et al.* [2006b] found that in air masses over Europe and the Mediterranean region, the single scattering albedo decreased sharply with wavelength from 0.91 ± 0.02 at 440 nm to 0.83 ± 0.04 at 1020 nm. *Xia et al.* [2005] reported that the average value for single scattering albedo did not change with wavelength, but that only the range of this change showed differences at different wavelengths.

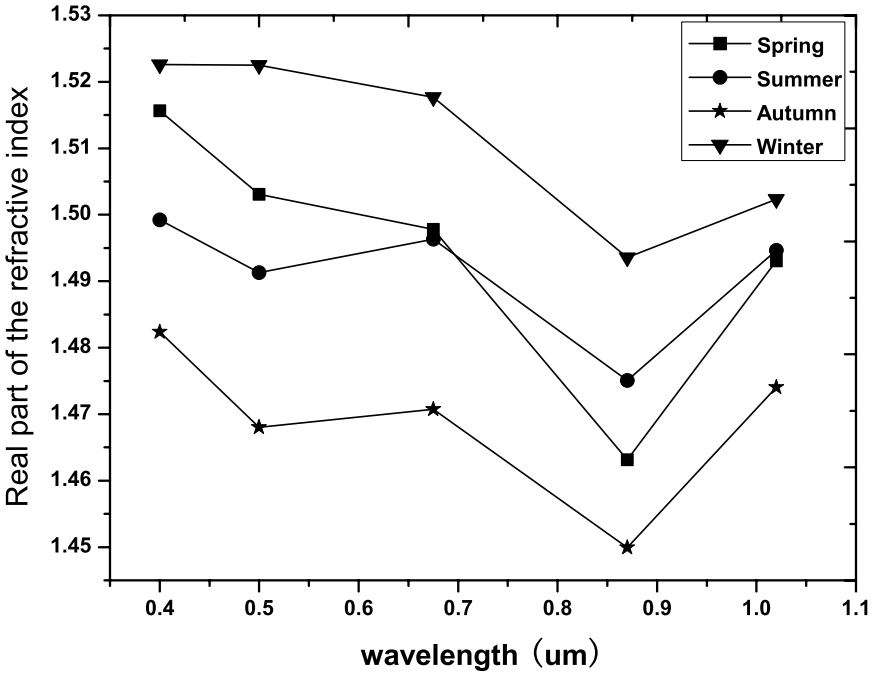

Figure 7. Seasonally averaged real part of aerosol refraction index at different wavelengths.

This study indicates that the single scattering albedo slightly increased with wavelength in spring, summer and autumn, but decreased with wavelength in winter. The above studies illustrate how the variation of the single scattering albedo with wavelength can be regional in nature.

4.4. Refractive Index

[24] Most of the information concerning the refractive index comes from aureole radiances, which are strongly affected by errors in the angle-pointing bias. The errors are estimated to be ±0.04 for the real part of the refractive index and 50% for the imaginary part of the refractive index. Figure 7 shows the seasonally averaged real part of the aerosol refraction index at 400, 500, 675, 870, and 1020 nm. The real part of the refractive index is less sensitive to wavelength in the 400–675 nm range and is more sensitive to wavelength in the 870–1020 nm range. *Yu et al.* [2006] and *Cheng et al.* [2006a, 2006b] found that in a given range

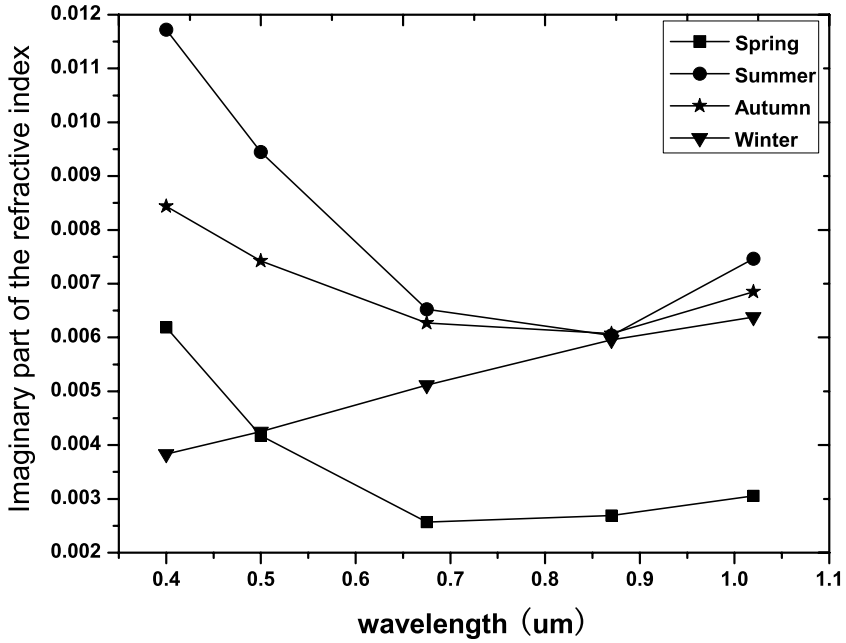

Figure 8. Seasonally averaged imaginary part of aerosol refraction index at different wavelengths.

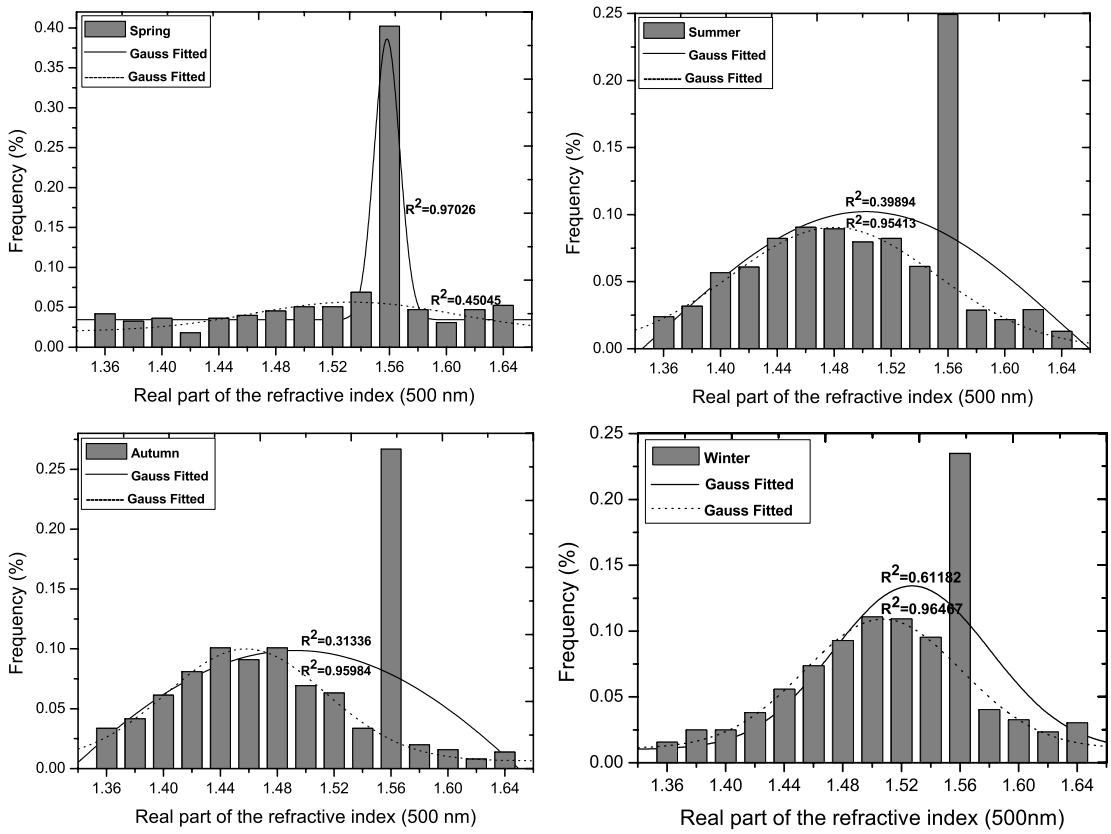

Figure 9. Frequency distributions of the real part of the aerosol refraction index for the four seasons and the fitted Gaussian model.

of AOT, the average value of the real part of the refractive index at higher wavelengths is larger than that at lower wavelengths because of the higher absorption in the near-infrared by coarse particles. In this study, the opposite was found, i.e., for all seasons, the maximum value of the real part of the imaginary index occurs at 400 nm and the minimum value occurs at 875 nm. Generally speaking, the real part of the refractive index is bigger in winter and smaller in autumn.

[25] The seasonally averaged imaginary part of the refractive index at 400, 500, 675, 870, and 1020 nm for the four seasons are shown in Figure 8. For the spring, summer and fall seasons, the imaginary part of the refractive index decreases with wavelength in the 400–675 nm range then slightly increases with wavelength in the 870–1020 nm range; maximum values occur at 400 nm. In winter, the imaginary part of the refractive index increases with wavelength, reaching a maximum value at 1020 nm. The average values of the imaginary part of the refractive index were 0.0037 (spring), 0.0082 (summer), 0.0070 (fall), and 0.0051 (winter).

[26] Figure 9 shows the frequency distribution of the real part of the aerosol refraction index at 500 nm for the four seasons. In general, the values range from 1.34 to 1.64, with the bulk of the values falling within the 1.54–1.56 range. In spring, more than 40% of the values for the real part of the aerosol refraction index ranged from 1.54 to 1.56. Nearly 25% of the values varied between 1.54–1.56 in the summer with other values during this season ranging from 1.38 to 1.54. For the fall season, approximately 27% of the values fell in the 1.54–1.56 interval, and more than 37% of values ranged between 1.4–1.48. More than 71% of the wintertime values varied between 1.44–1.56, and nearly 24% of the values ranged between 1.54–1.56.

[27] Little has been reported concerning the statistical characterizations of the real part of the aerosol refraction index until now. To gain further understanding, the frequency distributions of the real part of the aerosol refraction index were fit by a Gaussian model using two sets of data. The solid line in Figure 9 is the fit using all data and the dashed line is the fit using only those data falling outside the 21.54–1.56 range. Table 2 summarizes the seasonal statistics of the real part of the aerosol refraction index based on the fitted Gaussian models using the two sets of data. For the case when all data were used, the Gaussian model best describes the frequency distribution of the real part of the aerosol refractive index in the spring ($R^2 = 0.97026$). When data in the range of 1.54–1.56 were not considered, the Gaussian model offered the best fit for the frequency distribution of the real part of the aerosol refractive index in other seasons; the correlation coefficients were 0.95413, 0.95984, and 0.96467 in summer, autumn and winter, respectively. The seasonal variation of the frequency distribution of the real part of the aerosol refraction index might possibly provide a new way to estimate and characterize this quantity at locations near dust regions.

Table 2. Seasonal Statistics of the Real Part of the Aerosol Refraction Index Based on the Fitted Gaussian Models

	Gauss Fitted 1 Real Line				Gauss Fitted 2 Imagine Line			
	y_0	A	x_c	W	y_0	A	x_c	w
Spring	0.034 ± 0.005	0.008 ± 0.001	1.558 ± 0.002	0.017 ± 0.002	0.020 ± 0.013	0.006 ± 0.005	1.534 ± 0.017	0.141 ± 0.068
Summer	−0.123 ± 0.689	0.081 ± 0.406	1.502 ± 0.017	0.286 ± 0.582	0.0001 ± 0.008	0.016 ± 0.003	1.480 ± 0.004	0.144 ± 0.017
Autumn	−0.381 ± 5.176	0.279 ± 4.679	1.493 ± 0.020	0.463 ± 2.798	0.006 ± 0.004	0.013 ± 0.001	1.458 ± 0.003	0.112 ± 0.009
Winter	0.010 ± 0.022	0.017 ± 0.007	1.527 ± 0.011	0.107 ± 0.033	0.011 ± 0.004	0.013 ± 0.001	1.507 ± 0.003	0.107 ± 0.009

[28] A similar analysis was performed on the frequency distribution of the imaginary part of the refraction index, but no analytic function was found to best mathematically describe the data.

5. Conclusions

[29] The aerosol optical thickness (AOT), Angstrom exponent (α), volume size distributions, refraction index and single scattering albedo at Dunhuang (DH), a site located near a dust region in western China, were retrieved from January 1999 to March 2001 using the measurements made by a sky radiometer. The seasonal variation and statistical characteristics of these optical properties were studied.

[30] The AOT and α at this location varies with season and is mainly influenced by weather conditions, dust events and human activities. Larger AOT and smaller α appeared in spring, while smaller AOT and larger α appeared in autumn. The standard deviations were largest when the magnitudes of AOT and α were at their largest. The seasonal variation of the frequency distribution of AOT was consistent with the variation of seasonally averaged AOT over DH area. Because of the influence of dust events, the range of AOT values was larger in the spring than in autumn. The AOT frequency distributions were better approximated by lognormal distributions, especially in spring, which suggests that this is the appropriate distribution to use in areas located near dust regions. The seasonal variation of the frequency distribution of α indicated that most of the values in the springtime were smaller than in the fall. A Gaussian normal distribution best characterized the frequency distribution of α in spring. The relationship between α and AOT can be characterized by a simple exponential function for each season.

[31] The aerosol volume size distribution can be described by the sum of two lognormal distributions, and has two modes: an accumulation mode with a radius of 0.25 um, and a coarse mode with a radius of 7.7 um (maxima in spring and summer). A pseudomode with a radius of about 1.69 um located between the accumulation and coarse modes in spring is also present.

[32] The single scattering albedo showed a slight increasing trend with wavelength in spring, summer and autumn; the single scattering albedo in winter showed a decreasing trend with wavelength. The variation of single scattering albedo with wavelength has regional characteristics, which is corroborated by other studies. The single scattering albedo in spring was clearly higher than in other seasons, with an average value of 0.934. This mean value is lower than that reported by others for desert dust (0.95–0.99), which suggests the possible combination of dust, urban-industrial particles and biomass burning aerosols over DH.

[33] The real and the imaginary parts of the refraction index were bigger in winter and summer and smaller in autumn and spring. The maximum value for the real part of the refractive index occurred at 400 nm, and the minimum value occurred at 875 nm for all seasons. For all seasons, the real part of the aerosol refraction index varied between 1.34–1.64 with the bulk of the values falling within the 1.54–1.56 range. Two Gaussian model fits were generated using all data points for one fit and only those data points outside of the 1.54–1.56 range for the other fit; the greatest difference between the two fits was seen in the springtime. A representative statistical relationship for the frequency distribution of the imaginary part of the refraction index was not found.

[34] The statistical characteristics of the frequency distributions of AOT, α and the real part of the refractive index and the relationship between AOT and α might provide a way to identify and estimate the aerosol optical properties in areas located near dust regions.

[35] **Acknowledgments.** This work was supported by the National Basic Research Program of China (2006CB403705), also the NASA Radiation Science Program (NNX08AH71G) managed by Dr. Hal Maring. We thank Guangyu Shi, Institute of Atmospheric Physics, Chinese Academy of Sciences, for providing the direct and diffuse solar irradiance data from Dunhuang. We are grateful to the OpenCLASTR project for use of their "SKYRAD" package in this research. We also thank Maki Yamano, Center for Climate System Research, University of Tokyo, for her help in the running of the code.

References

AMS (2003), Climate change research issues for the atmospheric and related sciences, American Meteorological Society (AMS) executive summary, *Bull. Am. Meteorol. Soc., 84,* 508–515.

Behnert, I., V. Matthias, and R. Doerffer (2007), Aerosol climatology from ground-based measurements for the southern North Sea, *Atmos. Res.*, *84*, 201–220.

Charlson, R. J. (2000), Extending atmospheric aerosol measurements to the global scale, in *From Weather Forecasting to Exploring the Solar System*, edited by C. F. Boutron et al., pp. 2747–2764, EDP less Ulis, France.

Chen, H., X. Xia, P. Wang, and W. Zhang (2007), Ground-based measurements of aerosol optical properties and radiative forcing in North China, *China Particuology*, *5*, 202–207.

Cheng, T., H. Wang, Y. Xu, H. Li, and L. Tian (2006a), Climatology of aerosol optical properties in northern China, *Atmos. Environ.*, *40*, 1495–1509.

Cheng, T., Y. Liu, D. Lu, Y. Xu, and H. Li (2006b), Aerosol properties and radiative forcing in Hunshan Dake desert, northern China, *Atmos. Environ.*, *40*, 2169–2179.

D'almeida, G. A. (1987), On the variability of desert aerosol radiative characteristics, *J. Geophys. Res.*, *92*, 3017–3026.

Dubovik, O., B. N. Holben, T. F. Eck, A. Smimov, Y. J. Kaufman, M. D. King, D. Tanre, and I. Slutsker (2002), Variability of absorption and optical properties of key aerosol types observed in worldwide locations, *J. Atmos. Sci.*, *59*, 590–608.

Fouquart, Y., B. Bonnel, J. C. Brgniez, L. Buriez, L. Smith, and J. J. Morcrette (1987), Observation of Saharan aerosols: Results of ECLATS

Field experiment. Part II: Broadband radiative characteristics of the aerosols and vertical radiative flux divergence, *J. Clim. Meteorol.*, *25*, 38–52.
Hess, M., P. Koepke, and I. Schult (1998), Optical properties of aerosol and clouds: The software package OPAC, *Bull. Am. Meteorol. Soc.*, *79*, 831–844.
Holben, B. N., et al. (1998), AERONET—A federated instrument network and data archive for aerosol characterization, *Remote Sens. Environ.*, *66*, 1–16.
Holben, B. N., et al. (2001), An emerging ground-based aerosol climatology: Aerosol optical depth from AERONET, *J. Geophys. Res.*, *106*, 12,067–12,097.
Ignatov, A., and L. Stowe (2000), Physical basis, premises, and self-consistency checks of aerosol retrievals from TRMM VIRS, *J. Appl. Meteorol.*, *39*(12), 2259–2277.
IPCC (2001), Climate Change 2001: The scientific basis-contribution of Working Group I to the third assessment report of the Intergovernmental Panel on Climate Change, Cambridge Univ. Press, New York.
IPCC (2007), Climate Change 2007: The scientific basis-contribution of Working Group I to the fourth assessment report of the Intergovernmental Panel on Climate Change, Cambridge Univ. Press, New York.
Jacobson, M. Z. (2000), A physically-based treatment of elemental carbon optics: Implications for global direct forcing of aerosols, *Geophys. Res. Lett.*, *27*, 217–220.
Kaufman, Y. J., D. Tanre, O. Dubovik, A. Karnieli, and L. A. Remer (2001), Absorption of sunlight by dust as inferred from satellite and ground-based remote sensing, *Geophys. Res. Lett.*, *28*(8), 1479–1482.
Kaufman, Y. J., D. Tanre, and O. Boucher (2002), A satellite view of aerosols in the climate system, *Nature*, *419*, 215–223.
King, M. D., D. M. Byme, J. A. Reagan, and B. M. Herman (1980), Spectral variation of optical depth at Tucson Arizona between August 1975 and December 1977, *J. Appl. Meteorol.*, *19*, 723–732.
Koepke, P., M. Hess, I. Schult, and E. P. Shettle (1997), Global aerosol data set, *MPI Meteorol. Hamb. Rep*, pp. 243, 44.
Li, Z., F. Niu, K.-H. Lee, J. Xin, W. M. Hao, B. Nordgren, Y. Wang, and P. Wang (2007), Validation and understanding of MODIS aerosol products using ground-based measurements from the handheld sunphotometer network in China, *J. Geophys. Res.*, *112*, D22S07, doi:10.1029/2007JD008479.
Lyamani, H., F. J. Olmo, A. Alcantara, and L. Alados-Arboledas (2006), Atmospheric aerosols during the 2003 heat wave in southeastern Spain: Microphysical columnar properties and radiative forcing, *Atmos. Environ.*, *40*, 6465–6476.
Matthias, V., and J. Bosenberg (2002), Aerosol climatology for the planetary boundary layer derived from regular lidar measurements, *Atmos. Res.*, *63*, 221–245.
Nakajima, T., T. Tonna, R. Rao, P. Boi, Y. J. Kaufman, and B. Holben (1996), Use of sky brightness measurements from ground for remote sensing of particulate polydispersions, *Appl. Opt.*, *35*, 2672–2686.
O'Neill, N. T., and J. R. Miller (1984), Combined solar aureole and solar beam extinction measurements. 1: Calibration considerations, *Appl. Opt.*, *23*, 3691–3696.
O'Neill, N. T., A. Ignatov, B. N. Holben, and T. F. Eck (2000), The log-normal distribution as a reference for reporting aerosol optical depth statistics; empirical tests using multi-year, multi-site AERONET sunphotometer data, *Geophys. Res. Lett.*, *27*(20), 3333–3336.
Schmid, B., P. R. Spyak, S. F. Biggar, C. Wehrli, J. Sekler, T. Ingold, C. Matzler, and N. Kampfer (1998), Evaluation of the applicability of solar and lamp radiometric calibrations of a precision sun photometer operating between 300 and 1025 nm, *Appl. Opt.*, *37*, 3923–3941.
Schwartz, S. E., and M. O. Andrea (1996), Uncertainty in climate change caused by aerosols, *Science*, *272*, 1121–1122.
Shettle, E. P., and R. W. Fenn (1979), Models of aerosols of lower troposphere and the effect of humidity variations on their optical proprieties, *AFCRL Tech. Rep. 79 0214*, 100 pp., Air Force Cambridge Res. Lab., Hanscom Air Force Base, Mass.
Shiobara, M., T. Hayasaka, T. Nakajima, and M. Tanaka (1991), Aerosol monitoring using a scanning spectral radiometer in Sendai, Japan, *J. Meteorol. Soc., Jpn*, *69*, 57–70.
Smirnov, A., B. N. Holben, T. F. Eck, O. Dubovik, and I. Slutsker (2000), Cloud screening and quality control algorithms for the AERONET data base, *Remote Sens. Environ.*, *73*, 337–349.
Takamura, T., T. Nakajima, I. Okada, A. Uchiyama, N. Sugimoto, G. Shi, and J. Zhou (2002), Aerosol cloud-radiation study using the SKYNET data, The first ADEC Workshop, Tokyo, Japan http://www.aeoliandust.com.
Tanaka, M., T. Nakajima, and M. Shiobara (1986), Calibration of a sun-photometer by simultaneous measurements of direct-solar and circumsolar radiations, *Appl. Opt.*, *25*, 1170–1176.
Tonna, G., R. Rao, and T. Nakajima (1995), Aerosol features retrieved from solar aureole data: A simulation study concerning a turbid atmosphere, *Appl. Opt.*, *34*, 4486–4499.
Wang, Y., J. Xin, Z. Li, P. Wang, S. Wang, T. Wen, and Y. Sun (2006), AOD and Angstrom parameters of aerosols observed by the Chinese sun hazemeter Network from August to December 2004, *Environ. Sci.*, *27*(9), 1703–1711.
William, P., C. Petr, D. Mavendra, and M. Steven (2007), Trends in aerosol optical depth for cities in India, *Atmos. Environ.*, *35*(41), 7524–7532, doi:10.1016/j.atmosenv.2007.05.055.
WMO (1983), *Radiation Commission of IAPAM Meeting of Experts on Aerosol and Their Climatic Effects*, pp. 28–30, WCP55, Williamsburg, VA.
WMO (2001), *Strategy for the Implementation of the Global Atmosphere Watch Programme (2001–2007)*, WMO No. 142, pp. 43–45, World Meteorol. Organ., Geneva.
Xia, X., H. Chen, and P. Wang (2004), Aerosol properties in a Chinese semiarid region, *Atmos. Environ.*, *38*, 4571–4581.
Xia, X., P. Wang, H. Chen, G. Philippe, and W. Zhang (2005), Ground-based remote sensing of aerosol optical properties over north China in spring, *J. Remote Sens.*, *9*(4), 429–437.
Xin, J., Y. Wang, Z. Li, P. Wang, S. Wang, T. Wen, and Y. Sun (2006), Introduction and calibration of the Chinese Sun Hazemeter network, *Environ. Sci.*, *27*(9), 1697–1702.
Xin, J., et al. (2007), AOD and Angstrom parameters of aerosols observed by the Chinese Sun Hazemeter Network from August to December 2005, *J. Geophys. Res.*, *112*, D05203, doi:10.1029/2006JD007075.
Yu, X., T. Cheng, J. Chen, and Y. Liu (2006), A comparison of dust properties between China continent and Korea, Japan in East Asia, *Atmos. Environ.*, *40*, 5787–5797.

Z. Li, Department of Atmospheric and Oceanic Science and Earth System Science Interdisciplinary Center, University of Maryland, 2207 Computer and Space Sciences Bldg., College Park, MD 20782, USA.

J. Liu, R. Wu, and Y. Zheng, College of Environmental Science and Engineering, Nanjing University of Information Science and Technology, Number 219, Ning Liu Road, Nanjing 210044, China. (jianjun5212@hotmail.com; zhengyf@nuist.edu.cn)

T. Tamio, Center for Environmental Remote Sensing, Chiba University, 1-33, Yayoi-cho, Inage-ku, Chiba-shi, Chiba 263-8522, Japan.

B. Wang, LASG, Institute of Atmospheric Physics, Chinese Academy of Sciences, Beijing 100029, China.